THE ASTROPHYSICAL JOURNAL, 394:L29–L32, 1992 July 20

ON THE INCLUSION OF THE HYDROGEN DIMER IN THE ANALYSIS OF *VOYAGER* IRIS SPECTRA

BARBARA E. CARLSON,[1] QIANCHENG MA,[2] AND ANDREW A. LACIS[1]
Received 1992 March 9; accepted 1992 May 1

ABSTRACT

Empirical formulas are fitted to existing theoretical absorption spectra of H_2—H_2 pairs in the far-infrared allowing us to include dimer absorption, parameterized with the height dependence of the para-hydrogen profile, in our calculations. Comparison between synthetic and *Voyager* IRIS spectra shows that once the dimer absorption is included it is now possible to reproduce the hydrogen portion of the IRIS spectrum to within the precision of the measurements.

Subject heading: planets and satellites: individual: Jupiter

1. INTRODUCTION

The *Voyager* IRIS spectra of Jupiter are dominated by the collision-induced absorption from the $S_0(0)$ and $S_0(1)$ rotational lines of hydrogen. These broad absorption features are produced by free-free transitions in the translational continuum between pairs of H_2 molecules. Transitions between para levels, associated with even rotational quantum numbers, are responsible for the $S_0(0)$ line near 360 cm^{-1}, while transitions between ortho levels, associated with odd rotational quantum numbers, are responsible for the $S_0(1)$ line near 590 cm^{-1}. Radiatively the ortho and para states behave as a mixture of two separate gases, and since molecular hydrogen is the dominant source of thermal opacity, the *Voyager* IRIS spectra are thereby sensitive to both the value and the vertical distribution of para-hydrogen in the Jovian atmosphere.

Since transitions for which $\Delta J = 1$ are highly forbidden, a sample of pure H_2 that is rapidly cooled from temperatures in excess of 300 K tends to retain its 3:1 high-temperature "normal" para-hydrogen fraction of 0.25. However, in the presence of free-radical surface sites on NH_3 cloud particles, equilibration between ortho- and para-hydrogen is catalyzed resulting in the partial equilibration observed in the Jovian atmosphere (Massie & Hunten 1982).

Previous investigations of the *Voyager* IRIS observations have revealed that the Jovain para hydrogen fraction is not in thermodynamic equilibrium near the NH_3 cloud-top (Conrath & Gierasch 1983, 1984). This result implies that a vertical gradient exists between the cloud-top values measured by Voyager and the high-temperature equilibrium value of 0.25 at depth. Recently, Carlson, Lacis, & Rossow (1992, hereafter CLR) used the spectral dependence of the hydrogen absorption to retrieve the height dependence of the para-hydrogen profile. However, all of their synthetic spectra show noticeable departures from the observations in the 280–380 cm^{-1} spectral region. Although the magnitude of the difference between their synthetic spectra and the IRIS observations is small, being less than the standard deviation of the spectra within their ensembles, it is larger than the noise equivalent radiance of the measurements. Thus, this difference is meaningful and suggestive of the need for an improved treatment of atmospheric opacity in this spectral interval.

The sense of the spectral departure in the 280–320 cm^{-1} region is that the synthetic spectrum has too much absorption while in the 320–380 cm^{-1} region additional absorption is required. The change in sign of the spectral departure is important since the variation in absorption strength from the $S_0(0)$ line center to the line edge is used to retrieve the height dependence of the para-hydrogen profile. Since the absorption in the $S_0(0)$ line center is stronger than that in the wing, radiation in the line center originates at higher altitudes. As shown in CLR, radiation in the line center originates primarily above the NH_3 cloud and is thus unaffected by the presence of the cloud, while radiation in the wing originates deeper and is affected by the presence of the cloud. Thus, too much absorption in the 280–320 cm^{-1} region may be indicative of problems with the cloud parameterization, while the extra opacity needed near the $S_0(0)$ line center may be accounted for by the additional opacity provided by the dimer.

Frommhold, Samuelson, & Birnbaum (1984) have shown that the diminutive feature in the *Voyager* IRIS spectra near the $S_0(0)$ line center is due to the bound-free transitions of the hydrogen dimer. McKellar (1988) experimentally confirmed this identification. However, as in the CLR analysis, it has been common practice to include only the opacity provided by the free-free transitions between H_2 molecule pairs responsible for the broad $S_0(0)$ and $S_0(1)$ features.

Meyer, Frommhold, & Birnbaum (1989, hereafter MFB) have shown that the absorption arising from the free-bound (below 354 cm^{-1}) and bound-free (above 354 cm^{-1}) transitions of the hydrogen pairs can noticeably alter the continuum. MFB used first principles to calculate the rototranslational absorption spectra of H_2—H_2 pairs in the far-infrared. The detailed structure of the translational profile component (2023) or (0223) is rigorously included in their calculations. The good agreement between their theoretical results and existing experimental data indicates that their theory can be used to predict the hydrogen absorption spectrum over a wide range of temperature and frequency.

A more rigorous analysis of the fine structure of the dimer was performed by Schaefer (1987). In particular, Schaefer included potential anisotropy and allowed for centrifugal stretching, effects which alter the magnitude of the free-bound and bound-free absorptions but do not alter their ratio. Comparison between the results of MFB and Schaefer indicates

[1] Goddard Space Flight Center, Institute for Space Studies, 2880 Broadway, New York, NY 10025.
[2] Center for the Study of Global Habitability, Columbia University and Institute for Space Studies, Goddard Space Flight Center, New York, NY 10025.

that these differences are significant only when the structure of the dimer absorption is examined at high spectral resolution. However, at IRIS resolution (i.e., 4.3 cm^{-1}) these differences are quite small. Since we are interested in understanding the nature of the spectral departures found by CLR, and not explicitly in the analysis of the fine structure of the dimer, we use the MFB results.

Unfortunately, the MFB calculations are computationally expensive and therefore not practical for an extensive data analysis effort. Instead, empirical formulas, derived from their results, provide a fast and accurate means by which the observed dimer structure can be incorporated. We begin, in § 2, by fitting an empirical formula to the translational profile component (2023) of the MFB dimer structure for an equilibrium para-hydrogen fraction at 120 K. We then extend this profile component (2023) to temperature T and para-hydrogen fraction f_p following the temperature and para-hydrogen dependence of the MFB theory. By shifting this translational profile component to the resonance frequency of the $S_0(0)$ line, we obtain the dimer structure of the $S_0(0)$ line. This approach is justified since radiation near the $S_0(0)$ line center originates over a relatively small pressure interval corresponding to temperatures between 110 and 130 K (i.e., ≈ 120 K).

Finally, in § 3 we compare synthetic spectra calculated using this empirical formulation based on MFB's theoretical work with the best-fit synthetic spectrum shown in CLR for the Jovian North Equatorial Belt (NEB) hot spot ensemble. The excellent agreement between the synthetic and observed spectra strengthen CLR's conclusions of a height-dependent para-hydrogen profile and vertical association of the para-hydrogen gradient with the location of the NH_3 cloud. Moreover, inclusion of the dimer opacity and the use of the MFB results for the free-free continuum enable us to now reproduce the IRIS measurements to within the instrumental limitations.

2. DIMER FORMULATION

The dimer structures considered by MFB were calculated for a temperature T of 120 K and for an equilibrium ortho–to–para-hydrogen ratio. In this spectrum, two sharp peaks are located at $+2.6$ cm^{-1} and -2.6 cm^{-1} relative to the H_2 rotational transition frequencies. The peak at the positive frequency corresponds to the transition from the $l = 1$ bound state to the $l' = 2$ predissociating state and is smaller than the other located at the negative frequency which arises from the inverse transition, namely from the $l = 2$ predissociating state to the $l' = 1$ bound state, where l is the orbital angular quantum number of the dimer. Their intensity ratio is controlled by a factor $(1 - f_p)/(1 + f_p)$, as determined by the boson symmetry requirement, where f_p is the para-hydrogen fraction. MFB also noted the presence of a broader structure with the peak near $+12$ cm^{-1} corresponding to the transition from the $l = 0$ bound state to the $l' = 3$ predissociating state. Its broader partner located near -12 cm^{-1} is the inverse transition, i.e., from the $l = 3$ predissociating state to the $l' = 0$ bound state. The general shape of the transition at negative frequencies can be determined from the transition at positive frequency through the principle of detailed balance.

In their calculations, MFB use McConville's model (McConville 1981) for the potential function; thus, they omit the anisotropic components. However, since our goal is to generate synthetic spectra for comparison with the *Voyager* IRIS measurements, the effect of the anisotropic potential and its neglect, will be spectrally smeared out. Finally, modeling the dimer structure based on the calculations by MFB is justified given the radiometric precision of the IRIS instrument ($\approx 4 \times 10^{-9}$ W cm^{-2} sr^{-1}/cm^{-1} near 354 cm^{-1}).

Based on MFB, the absorption coefficient at temperature T and angular frequency $\omega = 2\pi c\nu$ arising from the rototranslational absorption spectra of H_2—H_2 pairs in the far-infrared region can be written as

$$\alpha(\omega, T) = \frac{2\pi^2}{3\hbar c} n^2 \omega (1 - e^{-\hbar\omega/kT}) V g(\omega, T) , \tag{1}$$

where n is the number density of the gas and V is the volume. In general, the spectral density $g(\omega, T)$ is a multiple sum of incoherent components designated by $\lambda_1\lambda_2\Lambda L$. Thus,

$$\begin{aligned} g(\omega, T) = \sum_{\lambda_1\lambda_2\Lambda L} \sum_{j_1 j_1' j_2 j_2'} & (2j_1 + 1) p_{j_1} c(j_1 \lambda_1 j_1', 000)^2 \\ & \times (2j_2 + 1) p_{j_2} c(j_2 \lambda_2 j_2', 000)^2 \\ & \times G_{\lambda_1\lambda_2\Lambda L}(\omega - \omega_{j_1 j_1'} - \omega_{j_2 j_2'}, T) \end{aligned} \tag{2}$$

following MFB, and using their notation, the spectrum is obtained by superposing base line profiles, i.e., translational profiles $G_{\lambda_1\lambda_2\Lambda L}$ are given by

$$\begin{aligned} V G_{\lambda_1\lambda_2\Lambda L}(\omega, T) = {} & \lambda_0^3 \hbar \sum_{ll'} (2l + 1) c(lLl'; 000)^2 \omega(ll' j_1 j_1' j_2 j_2') \\ & \times \left\{ \int_0^\infty \exp(-E_t/kT) dE_t |\langle l, E_t | B_{\lambda_1\lambda_2\Lambda L}(R) | l', E_t + \hbar\omega \rangle|^2 \right. \\ & + \sum_{n,n'} \exp(-E_{nl}/kT) |\langle l, E_{nl} | B_{\lambda_1\lambda_2\Lambda L}(R) | l', E_{n'l'} \rangle|^2 \delta(E_{n'l'} - E_{nl} - \hbar\omega) \\ & + \sum_{n} \exp(-E_{nl}/kT) |\langle l, E_{nl} | B_{\lambda_1\lambda_2\Lambda L}(R) | l', E_{nl} + \hbar\omega \rangle|^2 \\ & \left. + \sum_{n'} \exp[-(E_{n'l'} - \hbar\omega)/kT)] |\langle l, E_{n'l'} - \hbar\omega | B_{\lambda_1\lambda_2\Lambda L}(R) | l', E_{n'l'} \rangle|^2 \right\} , \end{aligned} \tag{3}$$

where $\lambda_0 = (2\pi\hbar^2/\mu kT)^{1/2}$ is the thermal de Broglie wavelength, $\omega(ll' j_1 j_1' j_2 j_2')$ is a weight factor which accounts for the molecular interchange symmetry, and $B_{\lambda_1\lambda_2\Lambda L}(R)$ are the components of the induced dipole moment. The most important components are the quadrupole-induced dipoles, $B_{2023}(R)$ and $B_{0223}(R)$, which account for about 98% of the collision-induced absorption rotational line intensity near the $S_0(0)$ line center. The right-hand side of equation (3) consists of four terms. The first term represents the free-free transitions and is the dominant term. The second term is the bound-bound transitions of the van der Waals dimers. The last two terms are the bound-free and free-bound transitions, respectively.

The dimer structure of the $S_0(0)$ line contains the contribution from the components $B_{2023}(R)$ and $B_{0223}(R)$, as calculated from the last two terms of equation (3). The theoretical results are in good agreement with the existing experimental data, indicating that the MFB theory can be used to predict the spectra over a wide range of temperature and frequency. However, since their theoretical calculations are complex and costly, this is not practical for all applications. In such cases, a simpler formalism, such as the EBC model (Borysow et al. 1985) which has been developed to model the theoretical results with a reasonable computer cost and a satisfactory accuracy, is more appropriate.

In this isotropic potential approximation, the dimer structure takes a simple form. If we included the anisotropic potential, as Schaefer (1987) did, the dimer structure would be more complex. However, for our application, where the theoretical

spectrum is convolved with the *Voyager* IRIS instrument function to a 4.3 cm^{-1} apodized resolution, the additional complexity is unnecessary.

We model the dimer structure predicted by MFB located in the positive frequency region with two empirical formulas, designated by $G^{1\to2}_{2023}(\omega, T_0, f_{p0})$ and $G^{0\to3}_{2023}(\omega, T_0, f_{p0})$, respectively, where the superscripts $1\to2$ and $0\to3$ indicate the related transitions and we also explicitly include the para-hydrogen fraction.

We then extend these formulas to temperature T and a specified para fraction following equation (3):

$$G^{1\to2}_{2023}(\omega, T, f_p) = \left(\frac{T_0}{T}\right)^{3/2} \exp\left[-\left(\frac{1}{kT}-\frac{1}{kT_0}\right)E_{l=1}\right]\frac{1-f_p}{1-f_{p0}}\,G^{1\to2}_{2023}(\omega, T_0, f_{p0})$$

$$G^{0\to3}_{2023}(\omega, T, f_p) = \left(\frac{T_0}{T}\right)^{3/2} \exp\left[-\left(\frac{1}{kT}-\frac{1}{kT_0}\right)E_{l=0}\right]G^{0\to3}_{2023}(\omega, T_0, f_{p0}), \quad (4)$$

where $E_{l=1}$ and $E_{l=0}$ are bound state energies.

As mentioned before, the inverse partners at negative frequencies can be obtained from the boson symmetry requirement and the detailed balance principle. The total spectrum is the sum of the basic line profile of the free-free transitions and the local contributions from the dimer structure of the $S_0(0)$ line modeled as described above. Due to the higher frequency structure of the dimer, the calculation of the dimer absorption is performed over a higher resolution wavenumber spacing then the absorption due to the free-free transitions. The free-free transitions are modeled at a frequency spacing of 5 cm^{-1}, while the dimer is included with a frequency spacing of 0.2 cm^{-1}.

3. RESULTS

The radiative transfer model used in this analysis is the same as that used in CLR but with the hydrogen opacity modeled as described above. Contributions from H_2—He collisions are included assuming a helium mole fraction of 0.12 (Gautier et al. 1981).

Following CLR, the spectral dependence of cloud extinction is obtained from Mie calculations, which are performed assuming a gamma size distribution (eq. [2.56] of Hansen & Travis 1974). As in CLR, the optical properties for NH_3 ice are taken from Martonchik, Orton, & Appleby (1984). In order to minimize the uncertainties associated with the parameterization of cloud extinction, we restrict this discussion to the North Equatorial Belt (NEB) hot spots since hot spots are regions of minimum, though not absence of, cloud opacity.

To calculate our synthetic spectrum, we use the best-fit model results from CLR. For the NEB hot spot ensemble, CLR found that the NH_3 cloud base forms at 0.5 bar above which the opacity is distributed following a particle-to-gas scale height ratio of 0.15. The total optical depth of the NH_3 cloud is 0.27 referenced at visible wavelengths ($\lambda = 0.5$ μm) with large particles providing $\tau = 0.19$. For this ensemble, the best-fit para-hydrogen profile is described by $P_L = 0.5 \pm 0.1$ bar, $P_U = 0.2 \pm 0.1$ bar, and $f_p = 0.32 \pm 0.01$ above 0.2 bar, where P_L and P_U are the lower and upper inflection points, respectively, specifying the gradient.

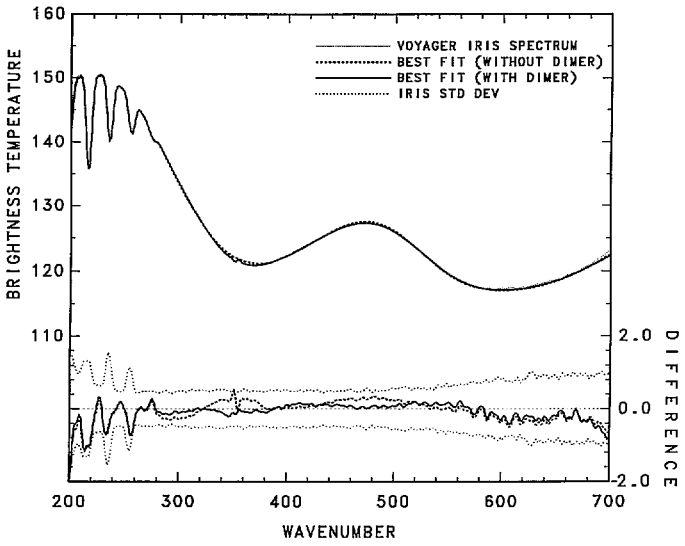

FIG. 1.—Comparison of our best-fit synthetic spectrum (*solid line*), the best-fit results of CLR (*dashed line*), and the average IRIS NEB hot spot spectrum (*dotted line*). The differences between the observed and synthetic spectra are shown in the lower portion of the figure along with the standard deviation of the individual IRIS spectra comprising the ensemble (*dotted lines*).

Figure 1 shows a comparison between our synthetic spectrum calculated including the dimer opacity (*solid line*), the best-fit results of CLR (*dashed line*), and the average IRIS NEB hot spot spectrum (*dotted line*). The differences between the synthetic and observed spectra are plotted in the lower portion of the figure along with the standard deviation of the individual IRIS spectra comprising the ensemble. It can be clearly seen that inclusion of dimer absorption significantly improves the agreement between the synthetic and observed spectra. Note that while the largest improvement is in the vicinity of the dimer feature near 350 cm^{-1}, there are significant contributions at other wavelength regions over the entire 300–500 cm^{-1} interval; these are attributable to the improvements in the calculation of the free-free continuum absorption with the new MFB formulation over the earlier version used in previous studies (e.g., CLR; Conrath & Gierasch 1983, 1984).

In summary, inclusion of the dimer absorption and the improved treatment for the collision-induced absorption associated with the free-free transitions clearly improves the quality of the model fit to the observed IRIS spectra. These results reinforce and confirm the height-dependent para-hydrogen profile previously retrieved by CLR. While the dimer structure should, in principle, provide additional constraints on the details of the height-dependent para-hydrogen profile, the 4.3 cm^{-1} spectral resolution of the IRIS measurements is not sufficiently high to fully resolve the dimer structure. Future high-resolution observations, such as those possible with Cassini CIRS, are required.

We thank R. Hanel and the *Voyager* IRIS team for designing such a capable instrument and obtaining one of the finest planetary data sets. We thank G. Orton and L. Frommhold for many helpful discussions and for supplying computer programs. We would like to acknowledge the support of the Planetary Atmospheres Discipline, NASA Office of Space Science and Applications.

REFERENCES

Borysow, J., Trafton, L., Frommhold, L., & Birnbaum, G. 1985, ApJ, 296, 644
Carlson, B. E., Lacis, A. A., & Rossow, W. B. 1992, ApJ, 393, 357 (CLR)
Conrath, B. J., & Gierasch, P. J. 1983, Nature, 306, 571
———. 1984, Icarus, 57, 184
Frommhold, L., Samuelson, R., & Birnbaum, G. 1984, ApJ, 283, L79
Gautier, D., Conrath, B., Flasar, M., Hanel, R., Kunde, V., Chedin, A., & Scott, N. 1981, J. Geophys. Res., 86, 8713
Hansen, J. E., & Travis, L. D. 1974, Space Sci. Rev., 16, 527
Martonchik, J. V., Orton, G. S., & Appleby, J. F. 1984, Appl. Opt., 23, 541
Massie, S. T., & Hunten, D. M. 1982, Icarus 49, 213
McConville, G. T. 1981, J. Chem. Phys., 74, 2201
McKellar, A. R. W. 1988, ApJ, 326, L75
Meyer, W., Frommhold, L., & Birnbaum, G. 1989, Phys. Rev. A, 39, 2434 (MFB)
Schaefer, J. 1987, ApJ, 182, L40